Journal of Materials Chemistry A

Accepted Manuscript

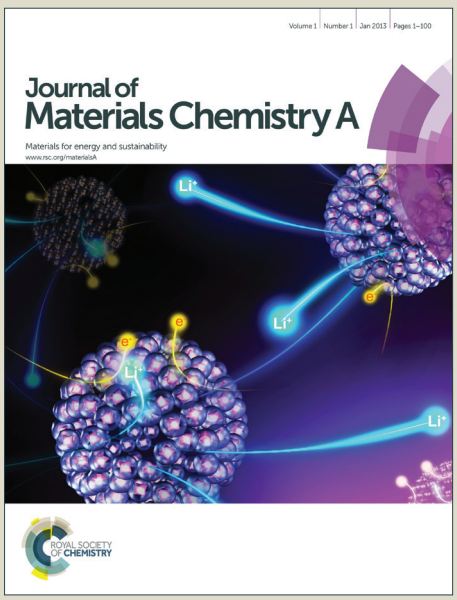

This is an *Accepted Manuscript*, which has been through the Royal Society of Chemistry peer review process and has been accepted for publication.

Accepted Manuscripts are published online shortly after acceptance, before technical editing, formatting and proof reading. Using this free service, authors can make their results available to the community, in citable form, before we publish the edited article. We will replace this *Accepted Manuscript* with the edited and formatted *Advance Article* as soon as it is available.

You can find more information about *Accepted Manuscripts* in the Information for Authors.

Please note that technical editing may introduce minor changes to the text and/or graphics, which may alter content. The journal's standard Terms & Conditions and the Ethical guidelines still apply. In no event shall the Royal Society of Chemistry be held responsible for any errors or omissions in this *Accepted Manuscript* or any consequences arising from the use of any information it contains.

ROYAL SOCIETY OF CHEMISTRY

www.rsc.org/materialsA

Journal of Materials Chemistry A RSCPublishing

ARTICLE

Non-covalent functionalization of reduced graphene oxide using sulfanilic acid azocromotrop and its application as supercapacitor electrode material

Cite this: DOI: 10.1039/xoxxoooooox

Received ooth January 2012,
Accepted ooth January 2012

DOI: 10.1039/xoxxoooooox

www.rsc.org/

Milan Jana,[a,b] Sanjit Saha,[a,b] Partha Khanra,[c] Pranab Samanta,[a] Hyeyoung Koo,[d] Naresh Chandra Murmu,[a] and Tapas Kuila[a,*]

Sulfanilic acid azocromotrop (SAC) modified reduced graphene oxide (SAC-RGO) was prepared through a simple non-covalent functionalization of graphene oxide (GO) followed by post reduction using hydrazine monohydrate. Spectral analysis (Fourier transform infrared, Raman and X-ray photoelectron spectroscopy) revealed the successful modification of graphene oxide with SAC through π-π interaction. The electrical conductivity of SAC-RGO was found to be ~ 551 S m^{-1}. The capacitive performance of SAC-RGO was recorded in a three electrode set up using 1 (M) aqueous H_2SO_4 as electrolyte. The -SO_3H functionalities of SAC contributed pseducapacitance as evidenced from the redox peaks (at ~ 0.43 and 0.27 V) appeared in the cyclic voltammetric (CV) curves of SAC-RGO. The contribution of electrical double layer capacitance was evidenced from the near rectangular shape CV curves and resulted a high specific capacitance of 366 F g^{-1} at a current density of 1.2 A g^{-1} for SAC-RGO electrode. An asymmetric device (SAC-RGO//RGO) was designed with SAC-RGO as positive electrode and RGO as negative electrode. The device showed an energy density of ~25.8 W h Kg^{-1} at a power density of ~980 W Kg^{-1}. The asymmetric device showed retention in specific capacitance of ~72% after 5000 charge-discharge cycles. The Nyquist data of the device was fitted with Z-View and different components (solution resistance, charge-transfer resistance and Warburg elements) were calculated from the fitted curves.

1. INTRODUCTION

The rapid growth of electrical vehicles and mobile electronic devices stimulates the demands for high energy storage resources. Electrochemical capacitors, supercapacitors or ultracapacitors have attracted enormous interest over the last decade due to its high energy and power density, low production cost and long term durability.[1] The supercapacitors are often hybridised with batteries and fuel cells to supply high power and energy harvesting applications. Supercapacitors are mainly classified in electrical double layered capacitors (EDLC) and pseudocapacitors (redox) according to their energy storage process.[2] However the real applications of supercapacitors are still restricted due to their inferior stored energy in comparison to the batteries.[2,3,4] Hence increasing specific capacitance and energy density without sacrificing life cycle is a matter of concern.

Graphene, a two dimensional monolayer of sp^2 hybridised carbon atoms decorated in a honeycomb crystal lattice has been regarded as an outstanding supercapacitor electrode material due to its high electrical conductivity, superior mechanical property, elevated theoretical surface area (2600 m^2 g^{-1}) and EDLC nature.[4] In comparison to other techniques, chemically derived graphene has drawn much attention towards the electrochemical charge storage applications due to its simple and cost effective production method.[5] However chemically derived graphene could be restacked due to their strong interlayer van der Waals forces and thus the specific surface area is reduced causing lower electrolyte penetration and ion accessibility.[6-8] Surface modification by using surface modifying agents or preparation of hierarchical composites is the effective method to prevent the agglomeration of graphene sheets. In most of the cases, the surface modifying agents or the newly added component is selected in such a way that they should contribute to enhance the specific capacitance via pseudocapacitance.[9] Various metal oxides like MnO_2, Co_3O_4, CuO, NiO, ZnO have been decorated as spacer materials in between the graphene sheets and extensively used as supercapacitor electrode materials.[10-14]Yu et al. have prepared sodium 4-aminoazobenzene-4-sulfonate modified graphene and used as supercapacitor electrode material. The functionalized graphene showed a specific capacitance of 210 F g^{-1}.[15] Lin et al. have prepared functionalized graphene by controlled solvothermal reaction and it showed a specific capacitance of 276 F g^{-1} at a current density of 0.1 A g^{-1}.[16] Jaidev et al. have shown that poly(p-phenylenediamine) modified exhibited a specific capacitance of 248 F g^{-1} at a current density of 2 A g^{-1}.[17] A large surface area

Journal of Materials Chemistry A Accepted Manuscript

graphene hydrogel was prepared by Luan et al.[18] The graphene hydrogel provided a specific capacitance of 232 F g^{-1} at 1 A g^{-1}.[18] Kumar et al. have used poly (3,4-propylenedioxythiophene) as a surface modifying agent and they got a specific capacitance of 201 F g^{-1} at a scan rate of 10 mV s^{-1}.[19] The sulfonated graphene/MnO_2/polyaniline ternary composite showed a specific capacitance of 276 F g^{-1} at 1 A g^{-1}.[20] Zang et al. have shown that N-doped graphene exhibits with a specific capacitance of 295 F g^{-1} at a current density of 5 A g^{-1}.[21] The specific capacitance of vapour mediated thermally exfoliated graphene has been found to be 175 F g^{-1} at a current density of 1 A g^{-1}.[22] In all these above cases, the funtionalization creates defects in the graphene surfaces as evidenced by the I_D/I_G (I_D=intensity of D band and I_G= intensity of G band) ratios from the Raman spectra analysis. In contrast, non-covalent functionalization via π-π interaction between graphene sheets and different stabilizers is the most useful alternative to tune the properties of graphene without altering its chemical construction.[23-25]

Energy density is a very important parameter of supercapacitor device and it can be calculated from the equation, $E = 1/2(CV^2)$. Here C is the specific capacitance and V is the potential window. In order to improve the energy density, the specific capacitance and the potential window should be increased simultaneously. There are two effective ways to improve the working potential of a supercapacitor device: (i) either by using organic/ionic electrolyte (ii) or by designing an asymmetric device. The organic/ionic electrolyte can provide a working potential over ~2 V.[26,27] However, the deterioration of specific capacitance of the electro active materials due to the low electrical conductivity of the non aqueous system is a major concern in supercapacitor applications.[26,27] The high production cost of the organic/ionic electrolyte is also inhibits its commercialization in energy storage device.[26,27] Therefore, the fabrication of asymmetric device with two different electro active materials is an alternative to achieve the cell voltage of ~ 2V by using aqueous electrolyte.[28-35]

Herein, we report the use of sulfanilic acid azo-cromotrop (SAC) as a surface modifying agent. It is anticipated to embed SAC on the graphene surface through π-π interaction. The -SO_3H functional groups of SAC were expected to provide the surface compatibility with the aqueous electrolyte and introduce pseudocapacitive nature in the modified graphene (SAC-RGO). We have designed an asymmetric supercapacitor device (SAC-RGO//RGO) with SAC-RGO and RGO as two different electro active materials. The capacitive performance of the device, SAC-RGO//RGO was evaluated through cyclic voltammetry (CV), charge-discharge and electrochemical impedance spectroscopy (EIS) analysis.

2. EXPERIMENTAL

2.1 Materials

Natural flake graphite was purchased from Sigma-Aldrich. Sulphuric acid, hydrogen peroxide, potassium permanganate and N, N-dimethyle formamide (DMF) were obtained from Merck, Mumbai, India. Polyvinylidene fluoride (PVDF) and Sulfanilic acid azo cromotrop was purchased from Sigma Aldrich. Conducting carbon black (EC-600JD, purity: >95%,) was purchased from Akzo Nobel Amides Co., Ltd, South Korea.

2.2 Preparation of surface modified graphene

Graphite oxide was prepared through modified Hummer's method as reported earlier.[23] About 100 mg of graphite oxide was dispersed in 100 ml of DI water by 30 minutes water bath sonication, followed by 5 minutes centrifugation at 6000 rpm to remove the un-exfoliated part and the clear brown dispersion of graphene oxide (GO) was taken in a 250 ml RB. About 0.3 g of SAC was dissolved in 100 ml of DI water and added drop wise to the GO dispersion with constant stirring using a bar magnet. The stirring was continued for ~24 h at room temperature afterwards 0.2 ml hydrazine monohydrate was added and refluxed for ~12 h at 100 °C. The mixture was cooled to room temperature and washed thoroughly by DI water with (pore size ≈ 0.1 μm) cellulose acetate membrane to remove the un-reacted SAC. The obtained black residue was dried in vacuum oven at 60 °C for 3 days and designated as SAC-RGO. The schematic for the preparation of SAC-RGO is shown in *Scheme 1*.

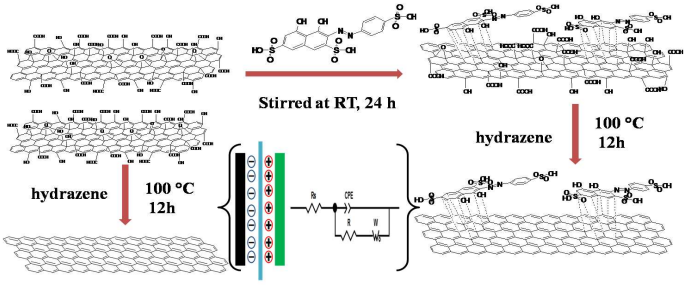

Scheme 1 Schematic for the preparation of SAC-RGO, RGO and supercapacitor device.

2.3 Structural and morphological characterization

Fourier transform infrared spectra (FT-IR) of pure GO and SAC-RGO were analysed by Nicolet iS10, Thermo scientific instrument, USA. The chemical environment of SAC-RGO was evaluated with X-ray photoelectron spectroscopy (XPS) by using a Kα x-ray photoelectron spectrometer, Tharmal scientific TM, USA. The defect content of the graphitic layers of SAC-RGO was measured by Raman spectra with Horiba Jobin Yvon, Kyoto, Japan. The morphology of the SAC-RGO was measured by Field emission scanning electron microscopy (FE-SEM) and transmission electron microscopy (TEM). FE-SEM was measured by Σigma HD, Carl Zeiss, Germany and TEM was recorded with JEOL-TEM 2100 (Japan) FS at 200 kV.

2.4 Electrical and electrochemical properties

Electrical conductivity was analysed by four probe method in a KEITHLEY Delta arrangement consisting of AC & DC current source, model: 6221 and Nanovoltmeter, model: 2182A. The electrical conductivity was calculated using the formula[36]

$$conductivity = \frac{1}{4.53 \times (I/V) \times d} \quad (1)$$

Where I is current (amp), V is voltage and d (metre) is the thickness of the pellet. In order to investigate the electrochemical analysis of SAC-RGO, the CV, galvanostatic charge-discharge and EIS were analysed with PARSTAT 4000 (Princeton Applied Research, USA) electrochemical workstation using 2 (N) H_2SO_4 as electrolyte. The SAC-RGO, carbon black and polyvinylidene fluoride were mixed homogenously with a mass ratio of 8:1.5:0.5 in dimethyle formamide. The slurry was then casted on the glassy carbon

Journal of Materials Chemistry A Accepted Manuscript

This journal is © The Royal Society of Chemistry 2012

working electrode. AgCl/Ag and Pt wire were used as the reference and the counter electrode, respectively. The deposited mass on the working electrode (glassy carbon) was ~ 0.1 mg.

Specific capacitance (SC) was determined by using the formula, $SC=I\times\Delta t/m\times\Delta V$.[23,36] Where I is for current, Δt is the discharging time, m is the active mass and ΔV is the potential window and m is the active mass. In order to verify the real application of SAC-RGO, an asymmetric supercapacitor device (1×1 cm^2) was designed using conducting carbon cloth support, where SAC-RGO and RGO were used as positive and negative electrode materials, respectively. The two carbon cloth supported electrodes were sandwiched in a supercapacitor cell, where whatman 42 filter paper was used as separator and 2 (N) H_2SO_4 as electrolyte. The SC of the asymmetric device was measured from the discharge curves using the equation,[28-35,37] $SC=I\times\Delta t/m\times\Delta V$, where the symbols bear same meaning as stated earlier. Energy density (E) and power density (P) can be calculated according to the formula, $E=1/2(CV^2)$ and $P=E/\Delta t$.[28-35,37] Where C is the specific capacitance, V is the operating voltage, Δt is the discharge time.

3. Results and Discussion

CV measurement is considered as the appropriate tool to distinguish between Faradic and non-Faradic type of energy storage mechanism.[38] Fig. 1 shows the comparative CV study of GO, RGO and SAC-RGO at 50 mV s^{-1} in the voltage range of -0.6 to 1 V. It was clearly revealed that SAC-RGO showed better current response than GO and RGO. The current response of GO is minimum due to its insulating nature and in case of RGO, the CV curve was nearly rectangular in shape, suggesting the EDLC nature of RGO. In contrast, the SAC-RGO showed strong intense redox peaks at ~ 0.43 and 0.27 V for anodic and cathodic scan, corresponding to the faradic reactions provided by the surface functionalities of SAC-RGO.
In order to find out the origin of capacitive performance of SAC-RGO a set of structural investigations, including FT-IR, Raman and XPS were investigated in detail. Fig. 2 shows the FT-IR spectra of GO, RGO, and SAC-RGO. Various oxygen functionalities were observed in the FT-IR spectrum of GO. The sharp peak at 1730 cm^{-1} was ascribed for the carboxyl (-COOH) group of GO.[23,36,39,40] The peak at 1220 and 1398 cm^{-1} were designated as the -C-OH stretching vibration and deformation vibration of -C-OH group, respectively.[23,36,39,40] The peak at 1064 and 1234 cm^{-1} were attributed to the stretching vibration peaks of alkoxy and epoxy, respectively.[23,36,39,40] The peaks related to the oxygen functionalities were almost absent in the FT-IR spectrum of RGO. The peak at ~ 1570 cm^{-1} in the spectrum of RGO and SAC-RGO was due to the restoration of C=C stretching bonds upon hydrazine reduction.[23,40] The peak at 1042 cm^{-1} in the spectrum of SAC was ascribed to the stretching vibration of –S=O of $-SO_3H$.[39,40] As observed from the spectrum of SAC-RGO, the -S=O bonds in SAC was still present with a small red shift to lower position at 1026 cm^{-1}. It may be due to the π-π stacking between RGO and SAC.[39,40] FT-IR spectra suggested that the appearance of redox peaks in the CV curve of SAC-RGO might be attributed to the $-SO_3H$ functionalities of SAC.

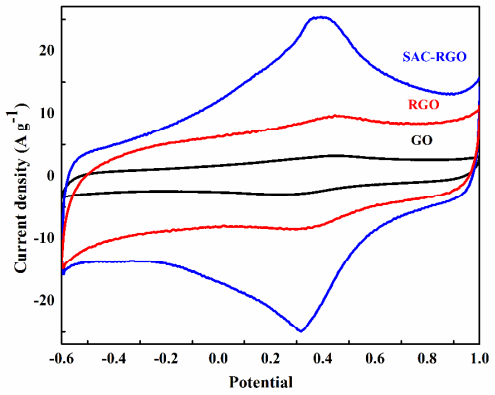

Fig. 1 CV of GO, RGO and SAC-RGO at 50 mV s^{-1}.

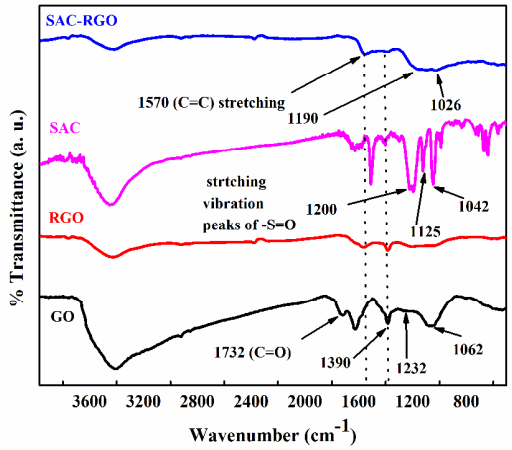

Fig. 2 FT-IR spectra of GO, RGO, SAC and SAC-RGO.

In order to further analyse the structure and chemical composition, XPS of GO, RGO and SAC-RGO were carried out. The deconvoluted C 1s spectra of GO (Fig. 3a) showed four different characteristic peaks at 284.0, 285.9, 286.4 and 288.0 eV which correspond to C-C/C=C bonds in the aromatic rings, C-O of alkoxy and epoxy, C=O of acidic and (carboxylic)/carbonyl, respectively.[23,36,39] It was seen that the oxygen functionalities were almost removed in the RGO as shown in Fig. 3(b), which was consistent with the FT-IR results. XPS spectra of SAC-RGO were represented in Fig. 3(c). The peaks corresponding to the oxygen functionalities were removed or decreased in the C 1s spectroscopy of SAC-RGO. Another peak at ~ 285.2 eV corresponding to C-N/C-S was observed in the C 1s spectra of SAC-RGO.[23,36,39] The increased peak intensity of C-C/C=C at ~ 284.2 in the C 1s spectra of SAC-RGO and RGO as compared with the GO suggested the restoration of π-electronic conjugated network structure after hydrazine reduction.[23,40-43] The S 2p and N 1s spectra of SAC-RGO were represented in Fig. 4(a) and 4(b), respectively. The S 2p peak at ~ 167.0 eV was due to the $-SO_3^-$ functionalities of SAC-RGO.[23,39,40] The N 1s peak at ~ 399 eV may be due to the -C-N bonds present in the SAC-RGO.[23,40,41] The XPS elemental analysis showed that SAC-RGO contains about 91% Carbon, 7% oxygen and 2% sulphur. The RGO contains about 92 % carbon and 8% oxygen, whereas GO

Journal of Materials Chemistry A Accepted Manuscript

contains 68% carbon and 32% of oxygen. Therefore, it is seen that most of the GO was reduced to RGO in the SAC-RGO.The results obtained from the XPS elemental analysis were also in line with the results obtained from the FT-IR spectra analysis.

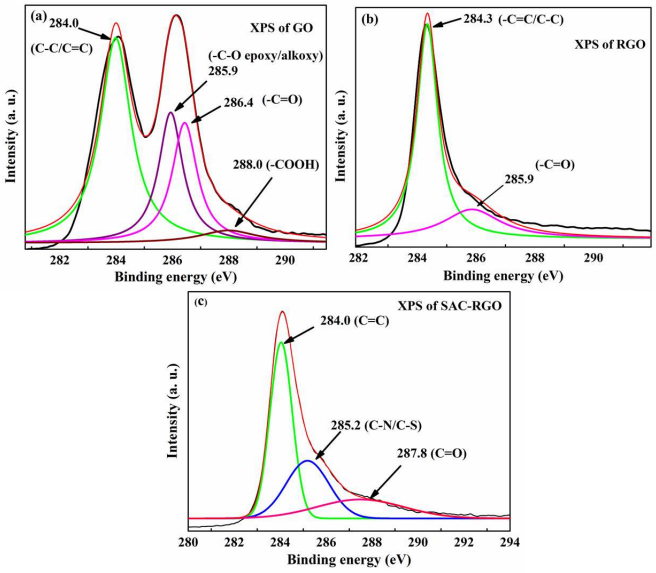

Fig. 3 C 1s XPS (a) GO, (b) RGO, (c) SAC-RGO.

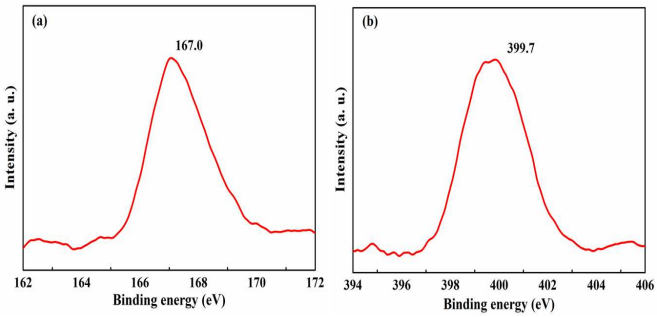

Fig. 4 (a) S 2p and (b) N 1s XPS of SAC-RGO.

Raman spectra can be used to obtain the structural information of RGO sheets in the SAC-RGO hybrids.[44-47] Raman spectra of RGO based composites consist of characteristic G and D bands at ~ 1584 and 1350 cm^{-1}, respectively. [44-47] Fig. 5 shows the Raman spectra of GO, RGO and SAC-RGO. It is seen that the G band of GO appeared at ~1585 cm^{-1} and the D band shifted to a lower region, which indicated the destruction of π-π* conjugated structure and formation of defects to the graphene layer because of extensive oxidation.[44-47] The formation of sp^3 bonds in the graphene moiety might cause low electrical conductivity.[9,36] The G and D band for RGO appeared at 1352 and 1592 cm^{-1}, respectively. In contrast, the G and D bands were appeared at 1590 and 1349 cm^{-1}, respectively for SAC-RGO. The shifting of G peak towards lower region in the RGO and SAC-RGO indicated the exfoliation of RGO sheets.[48] The changes in I_D/I_G (I_D = intensity of D band, I_G intensity of G band in Raman spectra) ratios can provide the information about the variable ratios of C_{sp3}/C_{sp2} of graphite moiety.[44-50] In case of GO, the I_D/I_G ratio was found to be 1.10, where as for RGO and SAC-RGO it was 0.92 and 0.97, respectively. In case of covalent functionalized graphene, the π-π* bonds may be interrupted.[39] Various modified graphene were reported with I_D/I_G > 1 confirming the existence of defects due to the formation of chemical bonds between the RGO sheets and surface modifying agents. A comparative study was carried out as shown in Table S1 (supporting information).

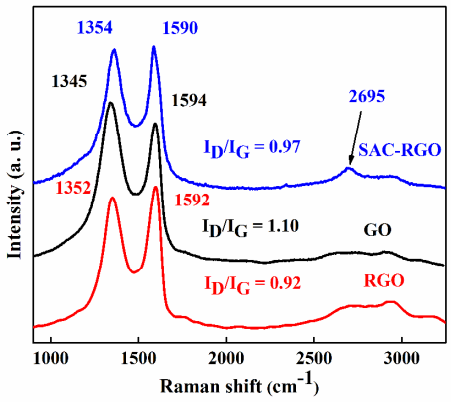

Fig. 5 Raman spectra of GO, RGO and SAC-RGO.

The low I_D/I_G ratios of SAC-RGO indicated that SAC interacts through its aromatic moiety with the basal plane of graphene (π-π stacking) without perturbing the conjugated sp^2 network of the honeycomb lattice.[51] It was worth noting that the basal arrangement of the graphitic domains was significantly improved, which was evaluated by its I_D/I_G ratios.[52] The 2 D band of graphene layers are very helpful to get idea about the number of layers in graphene.[46] The Raman spectra of SAC-RGO showed comparatively sharper 2D peak at ~ 2680 cm^{-1} signifying the formation of a-few-layers of functionalized RGO sheets.[23,46] On the other hand, a broad hump was formed at ~ 2750 cm^{-1} for RGO suggesting layer by layer stacking of RGO sheets during reduction.[44-48]

The morphological structure of SAC-RGO was measured by FE-SEM, TEM and selected area electron diffraction (SAED) pattern image analysis. Fig. 6 shows the FE-SEM images of SAC-RGO. The FE-SEM images exposed that layered structure of RGO can be maintained in the SAC-RGO after treating with hydrazine. Appearance of less aggregated sheets of SAC-RGO as compared to RGO confirmed the presence of hydrophilic functionalities (e.g., $-SO_3H$) of SAC in the surface modified graphene. The hydrophilic functionalities can prevent restacking of RGO sheets in the SAC-RGO resulting floppy and porous structure.[53] The porous nature of SAC-RGO can provide better penetration of electrolyte in the SAC-RGO electrode, resulting better current response of SAC-RGO than RGO in the CV analysis (Fig. 1). Thin two dimensional sheets were visible in the TEM image (Fig. 7a) of SAC-RGO with a huge amount of wrinkles; implying significant exfoliation of GO sheets during surface modification.[52] Fig. 7(b) represents the SAED pattern image of SAC-RGO. The appearance of ring pattern in the SAED pattern image of SAC-RGO suggested polycrystalline nature due to the overlapping of many RGO grains as evidenced from the TEM image.[54] It also may be due to the adsorption of SAC on the surface of RGO through π-π interaction.[55]

Journal of Materials Chemistry A Accepted Manuscript

This journal is © The Royal Society of Chemistry 2012

The restoration of conjugated π-π* bonds in the modified graphene was confirmed by electrical conductivity measurements. The electrical conductivity of GO was found to be ~9.1×10^{-4} S m^{-1}. The presence of various oxygen

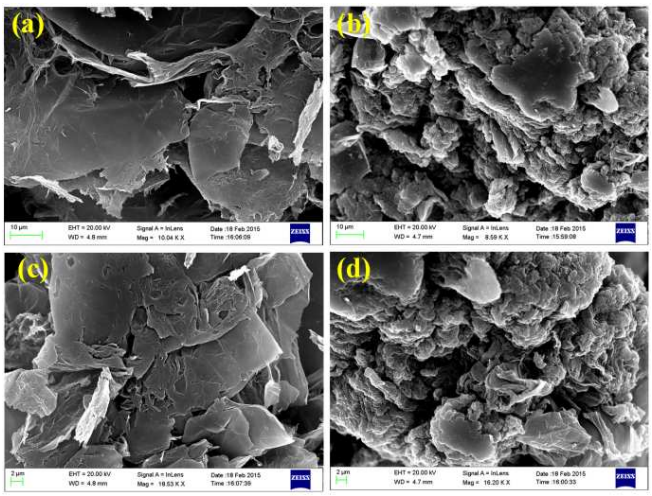

Fig. 6 FE-SEM images of (a,c) RGO and (b,d) SAC-RGO

functionalities might be responsible for its low electrical conductivity.[9,36,53] The electrical conductivity of RGO increased to 318 S m^{-1} and that of SAC-RGO it was found to be 551 S m^{-1}. This observation is in good agreement with the electrical conductivity of various surface modified graphene reported earlier as shown in Table S1 of supporting information. The low electrical conductivity of RGO as compared to SAC-RGO might be due to the restacking of RGO layers during reduction in absence of the surface modifying agents.[23] On the basis of these structural analysis, it was confirmed that GO was successfully modified with SAC and the pseducapacitance aroused in the CV analysis of SAC-RGO was mainly due to the -SO_3H functionalities of SAC-RGO. The proposed redox mechanism is shown in the *scheme 2*. It shows that the redox reaction is reversible in nature in the aqueous H_2SO_4 electrolyte. However, some extent of irreversibility due to the degradation of -SO_3H functionalities from SAC-RGO cannot be ruled out. There might be another quinine/hydroquinone transition during the electrochemical reactions which is very common for the carbonaceous materials [56-57]. The low current response of GO was due to the presence of non conducting oxygen functionalities. In case of RGO, the oxygen functionalities were more or less removed, but the π-π restacking caused lower conductivity, which might be responsible for its lower current response.[9,11]

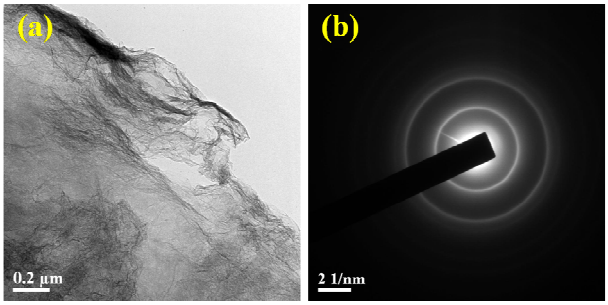

Fig.7 (a) TEM and (b) SAED pattern images of SAC-RGO

In order to check the supercapacitor application of SAC-RGO, CV at different scan rates were carried out in the voltage range of -0.6 to 1.0 V as shown in Fig. 8(a). SAC-RGO showed clear capacitive characteristics with rectangle-like CV curves. The curves maintained its redox peak-incorporated rectangular shape with increasing scan rates, signifying good wetting ability and easy access of ions to the electrode-electrolyte interfaces and fast charge-breeding capability of SAC-RGO. The appearances of redox peak-incorporated rectangular shape were the indication of both EDLC and pseducapacitance.[50,52] Also at high scan rates slight shifting of the anodic and cathodic peaks towards the positive and negative potential region suggested quasi-irreversible nature of the redox reactions provided by SAC-RGO composite.[26,40-41]

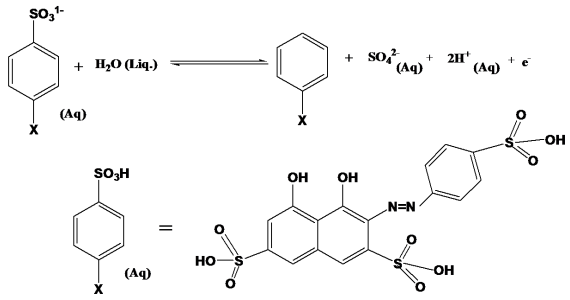

Scheme 2 Proposed redox mechanism during charging-discharging reaction on the SAC-RGO electrode in acidic medium

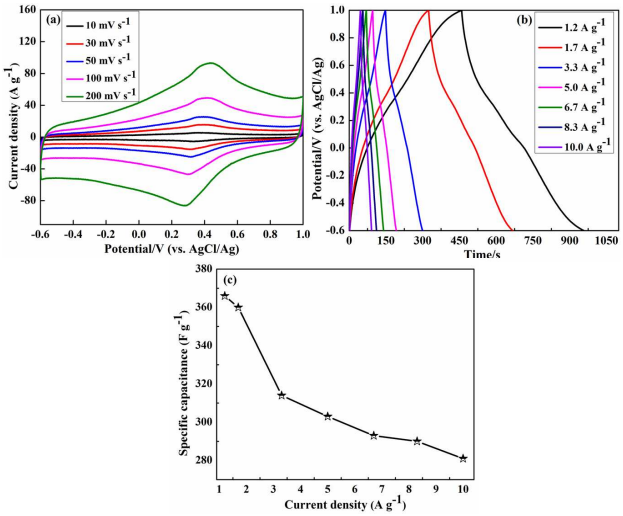

Fig. 8 (a) CV, (b) galvanometric charge-discharge and (c) SC vs current density plot of SAC-RGO in three electrode configurations.

Galvanostatic charge-discharge analysis was also conducted to measure the SC of SAC-RGO in three electrode system. Fig. 8(b) showed the galvanometric charge-discharge curve of SAC-RGO within the voltage range of -0.6 to 1 V at different current densities. The curves showed characteristic discharge plateau, which suggested that the existence battery like non-faradic (redox) nature.[38] The SC was found to be 366 F g^{-1} at a current density of 1.2 A g^{-1}. The dependence of SC on current density is shown in Fig. 8(c). Generally, the retention of SC with current density depends on; (i) diffusion of ions in electrolyte, (ii) adsorption of ions on the electrode and (iii) finally charge-transfer between electrode and electrolyte.[11,23] Any of the above

Journal of Materials Chemistry A Accepted Manuscript

mentioned condition might be slow at higher current density causing deterioration of SC.[11,23] About 76.7 % of its initial SC was retained when the current density increased from to 10 A g^{-1} indicating high rate capability of SAC-RGO.[11,52] A comparative study of recently developed similar kind of supercapacitor electrode materials has been summarized in the supporting information (Table S1). It is seen that the electrochemical properties of SAC-RGO were comparable or superior as compared to these modified graphene.

The CV curves of SAC-RGO showed the appearance of redox peaks in the positive region (~ 0.43 and 0.27 V). So, it is assumed that the SAC-RGO can be used as positive electrode of a supercapacitor device. A two electrode based asymmetric device was designed by using SAC-RGO as positive electrode, RGO as negative electrode (SAC-RGO//RGO) and carbon cloth as current collector. In order to fabricate the asymmetric device charge balance of the two electrodes was done from the characteristic CV curves (Fig. 1). The charge storage capacity (q) of an electrode depends on the working potential window, mass of the electrode (m) and the individual specific capacitance according the equation,[26-35] $q = SC \times m \times \Delta V$. In order to obtain charge balanced equation, $q_1 = q_2$, so, the mass ratio (m_2/m_1) can be calculated

$$\frac{m_2}{m_1} = \frac{\Delta V_1 \times SC_1}{\Delta V_2 \times SC_2}$$

(q_1 and q_2 were the charge storage capacity of RGO and SAC-RGO, respectively).

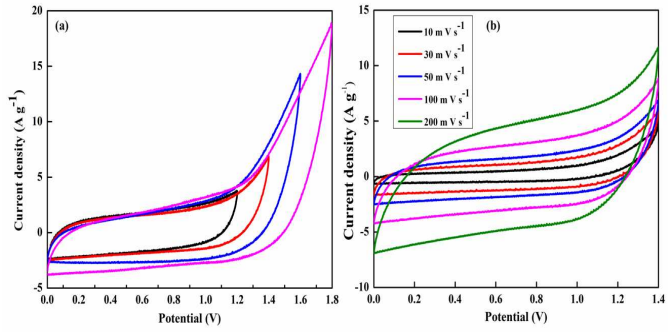

Fig. 9 (a) CV curves of SAC-RGO//RGO at different working potential at a scan rate of 50 mV s^{-1}, (b) CV curves of SAC-RGO//RGO at different scan rate.

The mass ratio of RGO to SAC-RGO was measured to be 1.96. The total mass of the active materials for the asymmetric device was ~ 1 mg (SAC-RGO = 0.337 mg and RGO = 0.663 mg). The electrochemical properties of the asymmetric device were measured by CV, charge-discharge and EIS. Fig. 9 (a) shows the CV curves of SAC-RGO//RGO in different voltage windows at 50 mV s^{-1} scan rate. It was observed that, SAC-RGO//RGO can provide a good capacitive performance with a quasi-rectangular CV profiles up to 0 to 1.4 V. So, the operation voltage window of 0-1.4 V was selected for SAC-RGO//RGO to analyse the electrochemical performances. CV analysis of SAC-RGO//RGO was analyzed with varying scan rate of 10-200 mV s^{-1} and the results are shown in Fig. 9 (b). It showed near rectangular nature of CV curves in the asymmetric system suggesting good capacitive behaviour. Fig. 10(a) shows galvanostatic charge-discharge curves of the asymmetric supercapacitor device. The variation of SC with current density is shown in Fig. 10(b). The SC of asymmetric device calculated as 95, 66.2, 57.2, 48.5, 43.7, 39.6, 34.3 and 32.3 F g^{-1} at current densities of 1.4, 2, 2.6, 3.2, 3.8, 4.4, 5.0 and 5.6 A g^{-1}, respectively. In order to validate the promising properties of the supercapacitor device, Ragone plot was analyzed as shown in Fig. 10(c). It showed that energy density reached to 25.86 W h Kg^{-1} at a power density of 980 W K g^{-1} and at high power density (3778 W Kg^{-1}), energy density decreased to 8.9 W h Kg^{-1}. A comparative analysis of asymmetric supercapacitor device with different electro active materials has been summarized in Table S2 of supporting information. It is seen that the energy density value of the current device is almost comparable to other materials as reported earlier [28-35]

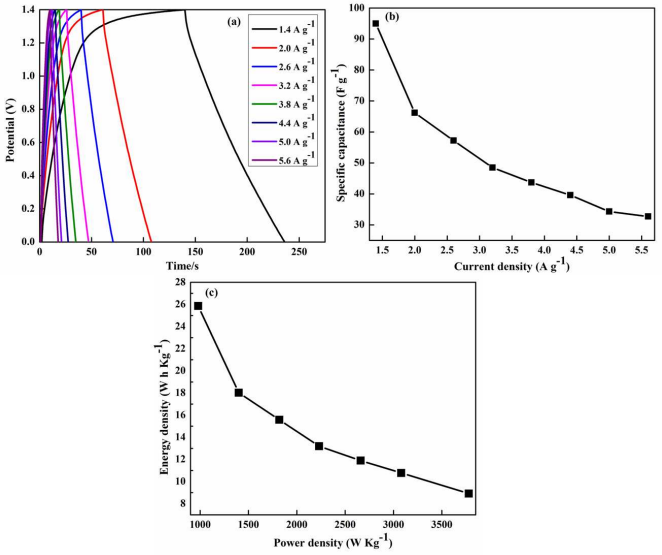

Fig. 10 (a) Galvanostatic charge-discharge curves of SAC-RGO//RGO at different current density (b) SC vs current density plot of SAC-RGO//RGO for asymmetric configuration and (c) Ragone plot (energy density vs. power density) of the asymmetric device.

A lengthy life cycle is an essential criterion for the real application of redox-EDLC hybrid supercapacitor.[52] Therefore; galvanostatic charge-discharge experiment was carried out up to 5000 cycles at a constant current density of 3.8 A g^{-1} as shown in Fig. 11(a). It is interesting to note that the SC value slightly increased during the early (~300 cycles) stages of the charge-discharge experiment. The initial improvement of SC at ~ 300 cycles might be due to the proper wetting of the electrode materials with the electrolyte.[11,23,53] The SC values started to decrease again after 400 cycles and retained ~72 % of its initial capacitance after 5000 cycles. It may be attributed to the irreversible redox reaction as explained in the proposed redox mechanism (*Scheme 2*) occurred during the charge-discharge reaction on the SAC-RGO electrode in acidic medium.

In order to observe properly the decrease of SC value with number of cycles, EIS was recorded after 0, 300, 1000 and 5000 cycles. Generally the Nyquist plot consists of a semicircle arch in the high frequency and a straight line in the low frequency region. Fig. 11 (b) showed the EIS curves at different number of cycles. The inset showed the corresponding equivalent Randles circuit of the Nyquist plot, which involves solution resistance (Rs), constant phase element (CPE), charge-transfer resistance (Rct) and Warburg element (W). The Z-

Journal of Materials Chemistry A Accepted Manuscript

This journal is © The Royal Society of Chemistry 2012

View fitted curves of the Nyquist plots are shown in the supporting information (Fig. S1, S2, S3 and S4). CPE can be expressed by CPE-T and CPE-P, where CPE-T is the capacitance and CPE-P is the constant phase element exponent.[58-62] The characteristic data obtained from Z-View fitting are summarised in Table 1.

The Warburg impedance (W) represents the route of ion diffusion from the electrolyte and can be divided in three parts: Ohmic resistance (W-R), diffusion time constant (W-T), and Warburg exponent (W-P).[59,62-65] The Rs of the device at first cycle was measured very low (0.68 Ω) signifying very good electrochemical contact of the electrode and electrolyte.[52]

The Rct formed due to the Faradic reactions and double layer capacitance was found to be 15.46 Ω, suggesting good charge-transfer characteristic of the SAC-RGO//RGOS.[62] The Rs and Rct values were consistent with the electrical conductivity measurement. The W-R (100 Ω) revealed the shorter ion diffusion path, which caused its good electrochemical properties.[63]

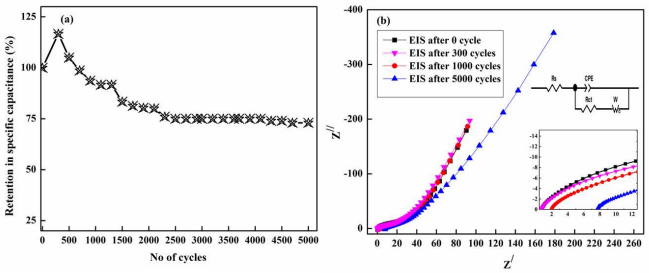

Fig. 11 (a) charge-discharge cyclic stability of SAC-RGO//RGO at 3.8 A g^{-1} current density (b) nyquist plot of SAC-RGO//RGO at different no of cycles. The inset shows the corresponding randles circuit of the nyquist plot from Z-view.

In general, the W-P for carbonaceous electrodes remained ~ 0.5-1 corresponding to the mass domain transport control of diffused ions from and to the electrolyte/electrode interface.[65,66] All the results obtained from the Z-View fitting of Nyquist plot showed that the device provided good capacitive performance.[4] Interestingly, it was found that the Rct and W-R were decreased to 12.2 and 95 Ω, respectively after 300 cycles. The decreased value of Rct and W-R after 300 cycles agreed well with the results obtained from the charge-discharge cyclic stability test. The Rs value of Nyquist plot was again increased to 1.87 Ω after 1000 cycles and became 6.7 Ω after 5000 charge-discharge cycles. It might be due to the loss of adhesion between active materials and current collectors and there might be possibilities of the current collectors being corroded by the electrochemical reactions taking part during charge-discharge cycles.[66] However, some extent of irreversibility due to the degradation of -SO_3H functionalities from SAC-RGO cannot be ruled out during charge-discharge cyclic stability, which may also affect the cyclic stability. The results obtained from the EIS were consistent with the charge-discharge stability curve. Therefore, it was seen that the SAC-RGO can be used as supercapacitors electrode material.

4. CONCLUSIONS

A highly conducting surface modified RGO was prepared through non-covalent functionalization technique. FT-IR, XPS and Raman study confirmed the successful surface modification of RGO using SAC. FT-IR was analysed to investigate the presence of -SO_3H functionalities in SAC-RGO. XPS was also utilized to analyse the chemical state of GO before and after surface modification followed by reduction. In comparison to GO and RGO, the high current response of SAC-RGO in the CV plots suggested its conducting nature which further confirmed by electrical conductivity measurement. The successful attachment of SAC on the RGO surfaces not only increased its electrical conductivity, but also added pseudo nature to the EDLC through the -SO_3H functionalities. The SAC-RGO electrode showed a high specific capacitance of 366 F g^{-1} at a current density of 1.2 A g^{-1}. A two electrode based asymmetric supercapacitor (SAC-RGO//RGO) was fabricated. The energy density was reached to 25.86 W h Kg^{-1} at a power density of 980 W Kg^{-1}. The EIS measurement was carried out with repeated charge-discharge cycles. The Z-View fitted data showed that the SC value was dependent on the R_S, R_{ct} and W-R. The designed device showed a good rate capability with retention in SC ~72 % after 5000 charge-discharge cycles. The very high electrochemical properties can be attributed to the redox reactions between -SO_3H/OH functionalities of SAC-RGO and the H^+ ions of H_2SO_4. Supercapacitors can be used in various fields of energy storage systems. Electrochemical supercapacitor finds several applications in portable electronic devices, elevator for emergency power supply, cold start-up of engine, backup power for airbag deployment, aerospace, electronic toys, etc. It can harvest power from braking systems and supply on demand in hybrid vehicles. It can also be used in blade pitch systems to improve the stability of energy grid.

Acknowledgements

Authors are also thankful to Department of Science and Technology, New Delhi, India for the financial supports vide DST-INSPIRE Faculty Scheme (IFA12-CH47) - INSPIRE Programme and Council of Scientific and Industrial Research, New Delhi, India for funding MEGA Institutional project (ESC0112/RP-II).

Notes and references

[a] *Surface Engineering & Tribology Division, Council of Scientific and Industrial Research-Central Mechanical Engineering Research Institute, Durgapur -713209, India*

[b] *Academy of Scientific and Innovative Research (AcSIR), Anusandhan Bhawan, 2 Rafi Marg, New Delhi-110001, India*

[c] *Soft Innovative Materials Research Centre, Korea Institute of Science and Technology (KIST) Jeonbuk 565905, South Korea*

[d] *Soft Innovative Materials Research Centre, Institute of Advanced Composite Materials, Korea Institute of Science and Technology (KIST) Jeonbuk 565905, South Korea*

*Correspondence to: Dr. Tapas Kuila (E-mail:tkuila@gmail.com; Phone: +919647205077)

REFERENCES

1. R. K¨otz, M. Carlen, *Electrochim. Acta*, 2000, **45**, 2483.
2. H. P. Cong, X. Chen Ren, P. Wang, S. H. Yu, *Energy Environ. Sci.*, 2013, **6**, 1185.
3. T. Chen, L. Dai, *J. Mater. Chem. A*, 2014, **2**, 10756.

Journal of Materials Chemistry A Accepted Manuscript

4. N. Xiao, H. Tan, J. Zhu, L. Tan, X. Rui, X. Dong, Q. Yan, *ACS Appl. Mater. Interfaces,* 2013, **5**, 9656.
5. M. Segal, *Nat. Nano*, 2009, **4**, 612.
6. Q. Wu, Y. X. Xu, Z. Y. Yao, A. R. Liu, G. Q. Shi, *ACS Nano,* 2010, **4**, 1963.
7. Z.-F. Li, H. Zhang, Q. Liu, L. Sun, L. Stanciu, J. Xie, *ACS Appl. Mater. Interfaces,* 2013, **5**, 2685.
8. Z. Lei, F. Shi, L. Lu, *ACS Appl. Mater. Interfaces,* 2012, **4**, 1058.
9. T. Kuila, S. Bose, A. K. Mishra, P. Khanra, N. H. Kim, J. H. Lee, *Prog. Mater. Sci.*, 2012, **57**, 1061.
10. S. Chen, J. Zhu, X. Wu, Q. Han, X. Wang, *ACS-nano*, 2010, **4**, 2822.
11. C. Xiang, M. Li, M. Zhi, A. Manivannan, N. Wu, *J. Power Sources*, 2013, **226,** 65.
12. K. K. Purushothaman, B. Saravanakumar, I. M. Babu, B. Sethuraman, G, Muralidharan, *RSC Adv.*, 2014, **4**, 23485.
13. C. Wang , J. Xu , M. F. Yuen , J. Zhang, Y. Li , X. Chen , W. Zhang, *Adv. Funct. Mater.* 2014, **24**, 6372.
14. Z. Li, Z. Zhou, G. Yun, K. Shi, X. Lv, B. Yang, *Nanoscale Res. Letters,* 2013, **8**, 473.
15. D. S. Yu, T. Kuila, N. H. Kim, P. Khanra, J. H. Lee, *Carbon*, 2013, **54**, 310.
16. Z. Lin, Y. Liu, Y. Yao, O. J. Hildreth, Z. Li, K. Moon, C. Wong, *J. Phys. Chem. C*, 2011, **115**, 7120.
17. Jaidev, S. Ramaprabhu, *J. Mater. Chem.,* 2012, **22**, 18775.
18. V. H. Luan, H. N. Tien, L. T. Hoa, N. Thi M. Hien, E.-S. Oh, J. S. Chung, E. J. Kim, W. M. Choi, B.-S. Kong, S. H. Hur, *J. Mater. Chem. A*, 2013, **1**, 208.
19. N. A. Kumar, H. J. Choi, A. Bund, J.-B. Baek, Y. T. Jeong, *J. Mater. Chem.*, 2012, **22**, 12268.
20. G. Wang, Q. Tang, H. Bao, X. Li, G. Wang, *J. Power Sources,* 2013 **241**, 231.
21. H. Zhang, T. Kuila, N. H. Kim, D. S. Yu, J. H Lee, *Carbon*, 2014, **69**, 66.
22. Y. Yan, T. Kuila, N. H. Kim, J. H. Lee, *Carbon,* 2014, **74,** 195.
23. M. Jana, P. Khanra, N. C. Murmu, P. Samanta, J. H. Lee, T. Kuila, *Phys. Chem. Chem. Phys.,* 2014, **16**, 7618.
24. S. Bose, T. Kuila, A. K. Mishra, N. H. Kim, J. H. Lee, *Nanotechnol.,* 2011, **22** 405603.
25. H. Bai, Y. Xu, L. Zhao, C. Li, G. Shi, *Chem. Commun*., 2009, **1667**,1667.
26. M. Kim, J. Kim, *Phys. Chem. Chem. Phys.,* 2014, **16**, 11323.
27. Y. Hou, L. Chen, P. Liu, J. Kang, T. Fujita, M. Chen, *J. Mater. Chem. A*, 2014, **2**, 10910.
28. J. Cao, Y. Wang, Y. Zhou, J. H. Ouyang, D. Jia, L. Guo, *J. Electroanal. Chem*. 2013, **689**, 201.
29. H. Gao, F. Xiao, C. B. Ching, H. Duan, *ACS Appl. Mater. Interfaces*, 2012, **4**, 7020.
30. D. Antiohosa, K. Pingmuangb, M. S. Romanoa, S. Beirnea, T. Romeoa, P. Aitchisonc, A. Minettd, G. Wallacea, S. Phanichphantb, J. Chena, *Electrochim. Acta* 2013, **101**, 99.
31. J. Shen, C. Yang, X. Li, G. Wang, *ACS Appl. Mater. Interfaces,* 2013, **5**, 8467.
32. H. Wang, Y. Liang, T. Mirfakhrai, Z. Chen, H. S. Casalongue, H. Dai, *Nano Res*. 2011, **4**, 729.
33. S. Wu, W. Chen, L. Yan, *J. Mater. Chem. A*, 2014, **2**, 2765.
34. C. Yang, J. Shen, C. Wang, H. Fei, H. Bao, G. Wang, *J. Mater. Chem. A*, 2014, **2**, 1458.
35. H. Wang, H. Yi, X. Chen, X. Wang, *J. Mater. Chem. A*, 2014, **2**, 3223.
36. M. Jana, S. Saha, P. Samanta, N. C. Murmu, J. H. Lee, T. Kuila, Mater. Chem. Phys., doi:10.1016/j.matchemphys.2014.11.037.
37. X. Yang, F. Zhang, L. Zhang, T. Zhang, Y. Huang, Y. Chen, *Adv. Funct. Mater.* 2013, **23**, 3353.
38. L. Li, Y. Zhang, F. Shi, Y. Zhang, J. Zhang, C. Gu, X. Wang, J. Tu, *ACS Appl. Mater Inter.*, 2014, **6,** 18040.
39. Y. Yan, T. Kuila, N. H. Kim, B.-C. Ku, J. H. Lee, *J. Mater. Chem. A*, 2013, **1**, 5892.
40. F. Li, Y. Bao, J. Chai, Q. Zhang, D. Han, L. Niu, *Langmuir*, 2010, **26**, 12314.
41. Y. Chang, G. Han, J. Yuan, D. Fu, F. Liu, S. Li, *J. Power Sources*, 2013, **238**, 492.
42. V. H. Luan, H. N. Tien, L. T. Hoa, N. T. M. Hien, E.-S. Oh, J. S. Chung, E. J. Kim, W. M. Choi, B.-S. Kong, S. H. Hur, *J. Mater. Chem. A*, 2013, **1**, 208.
43. T. Kuila, S. Bose, P. Khanra, A. K. Mishra, N. H. Kim, J. H. Lee, *Carbon*, 2012, **50**, 914.
44. D. Yang, A. Velamakanni, G. Bozoklu, S. Park, M. Stoller, R. D. Piner, S. Stankovich, I. Jung, D. A. Field, C. A. Ventrice, R. S. Ruoff, , *Carbon*, 2009, **47**, 145.
45. K. N. Kudin, B. Ozbas, H. C. Schniepp, R. K. Prud'homme, I. A. Aksay, R. Car, *Nano Lett*., 2008, **8**, 36.
46. A. C. Ferrari, *Solid State Commun,* 2007, **143**, 47.
47. A. C. Ferrari, J. C. Meyer, V. Scardaci, C. Casiraghi, M. Lazzeri, F. Mauri, S. Piscanec, D. Jiang, K. S
48. B. R. Duan, Q. Cao, *Electrochim. Acta*, 2012, **64**, 154.
49. M. Toupin, T. Brousse, D. Bélanger, *Chem. Mater.* 2002, **14**, 3946.
50. C. Yu, P. Ma, X. Zhou, A. Wang, T. Qian, S. Wu, Q. Chen, *ACS Appl. Mater. Inter.*, 2014, **6**, 17937.
51. V. K. Kodali, J. Scrimgeour, S. Kim, J. H. Hankinson, K. M. Carroll, W. A. Heer, C. Berger, J. E. Curtis, *Langmuir*, 2011, **27**, 863.
52. Y. Fang, B. Luo, Y. Jia, X. Li , B. Wang, Q. Song, F. Kang, L. Zhi, *Adv. Mater*. 2012, **24**, 6348.
53. W. Ai, W. Zhou, Z. Du, Y. Du, H. Zhang, X. Jia, L. Xie, M. Yi,.T. Yu, W. Huang, J. *Mater. Chem.*, 2012, **22**, 23439.
54. D. Chen, L. Li, L. Guo, *Nanotechnology,* 2011, **22**, 325601.

Journal of Materials Chemistry A Accepted Manuscript

This journal is © The Royal Society of Chemistry 2012

55. P. Liu, Y. Huang, L. Wang, W. Zhang, *J. Alloy. Compd*., 2013, **573**, 151.
56. K. Fic, E. Frackowiak, F. Beguin, *J. Mater. Chem.,* 2012, **22**, 24213.
57. K. G. Gallagher, T. F. Fuller, *Phys. Chem. Chem. Phys*., 2009, **11**, 11557.
58. R. Farma, M. Deraman, Awitdrus, I. A. Talib, R. Omar, J. G. Manjunatha, M. M. Ishak, N. H. Basri, B. N. M. Dolah, *Int. J. Electrochem. Sci.*, 2013**, 8**, 257.
59. L. Oakes, A. Westover, J. W. Mares, S. Chatterjee, W. R. Erwin, R. Bardhan, S. M. Weiss, C. L. Pint , *Sci. Rep*. 2013, **3,** 3020.
60. J. Backholm, P. Georén, G. A. Niklasson, *J. Appl. Phys*, 2008, **103**, 023702.
61. A. Ramadoss , S. J. Kim, *Mater. Chem. Phys.* 2013, **140,** 405.
62. N. Zhu, W. Liu, M. Xue, Z. Xie, D. Zhao, M. Zhang, J. Chen, T. Cao, *Electrochim. Acta*, 2010, **55**, 5813.
63. J. Song, M. Z. Bazant, *J. Electrochem. Soc.* 2013, **160**, A15.
64. A. Ehsani, M. G. Mahjani, M. Jafarian, *T. J. Chem*, 2011, **35**, 735.
65. M. Y. Ho, P. S. Khiew, D. Isa, T. K. Tan, W. S. Chiu, C. H. Chia, M. A. A. Hamid, R. Shamsudin, *Sains Malays.* 2014, **43**, 885.
66. Y. Zhu, C. Cao, S. Tao, W. Chu, Z. Wu, Y. Li, *Sci. Rep.* 2014, **4,** 5787.

Journal of Materials Chemistry A Accepted Manuscript

Table 1. Fitted values of R_S, Rct, CPE-T, CPE-R, W-R, W-T, W-P from the equivalent circuit corresponded to Figure S1, S2, S3, S4

EIS at different no of charge-discharge cycles	Rs (Ω)	CPE-T	CPE-P	Rct (Ω)	W-R	W-T	W-P
After 0 cycle	0.68	0.0005	0.7	15.4	100	0.7	0.49
After 300 cycles	0.68	0.0005	0.7	12.2	95	0.68	0.5
After 1000 cycles	1.87	0.0005	0.7	15.1	98	0.7	0.5
After 5000 cycles	6.7	0.005	0.4	24	135	0.35	0.5

Journal of Materials Chemistry A Accepted Manuscript